Stem Cell Reports

Article

Enhancing the Efficacy of Stem Cell Therapy with Glycosaminoglycans

Ling Ling,[1,8] Xiafei Ren,[2,8] Xue Cao,[2,7] Afizah Binte Mohd Hassan,[2] Sophia Mah,[1]
Padmapriya Sathiyanathan,[1] Raymond A.A. Smith,[1] Clarissa L.L. Tan,[1] Michelle Eio,[1]
Rebekah M. Samsonraj,[1,6] Andre J. van Wijnen,[3] Michael Raghunath,[4,5] Victor Nurcombe,[1] James H. Hui,[2,*]
and Simon M. Cool[1,2,*]

[1]Institute of Medical Biology, Agency for Science Technology and Research (A*STAR), 8A Biomedical Grove, #06-06 Immunos, Singapore 138648, Singapore
[2]Department of Orthopaedic Surgery, Yong Loo Lin School of Medicine, National University Health System, National University of Singapore, 1E Kent Ridge Road, Singapore 119074/119288, Singapore
[3]Department of Orthopaedic Surgery & Biochemistry and Molecular Biology, Mayo Clinic, Rochester, MN 55905, USA
[4]Department of Biochemistry, Yong Loo Lin School of Medicine, National University of Singapore, Singapore 117596, Singapore
[5]Present address: Institute for Chemistry and Biochemistry, School of Life Sciences and Facility Management, Zurich University of Applied Sciences (ZHAW), 8820 Wädenswil, Switzerland
[6]Present address: Department of Medicine, Mayo Clinic, Rochester, MN, USA
[7]Deceased 20 May 2019
[8]Co-first author
*Correspondence: james_hui@nuhs.edu.sg (J.H.H.), simon.cool@imb.a-star.edu.sg (S.M.C.)
https://doi.org/10.1016/j.stemcr.2019.12.003

SUMMARY

Human mesenchymal stem cell (hMSC) therapy offers significant potential for osteochondral regeneration. Such applications require their *ex vivo* expansion in media frequently supplemented with fibroblast growth factor 2 (FGF2). Particular heparan sulfate (HS) fractions stabilize FGF2-FGF receptor complexes. We show that an FGF2-binding HS variant (HS8) accelerates the expansion of freshly isolated bone marrow hMSCs without compromising their naivety. Importantly, the repair of osteochondral defects in both rats and pigs is improved after treatment with HS8-supplemented hMSCs (MSC[HS8]), when assessed histologically, biomechanically, or by MRI. Thus, supplementing hMSC culture media with an HS variant that targets endogenously produced FGF2 allows the elimination of exogenous growth factors that may adversely affect their therapeutic potency.

INTRODUCTION

Osteochondral defects are complicated by the involvement of not only subchondral bone but an avascular superficial layer of cartilage with low cellularity (Huang et al., 2016). Treatment strategies have included micro-fracture, osteochondral grafts, and autologous chondrocyte implantation (Grande et al., 1989; Mahmoud et al., 2017). However, micro-fracture is limited by the suboptimal release of viable cells and rapid clearance of mobilized growth factors, leading to fibrocartilage deposits and inadequate subchondral bone regeneration (Kon et al., 2009). Outcomes following osteochondral grafting are also variable due to poor graft/host integration (Bentley et al., 2012). Although the limited growth potential of chondrocytes and their rapid functional loss *ex vivo* (Darling and Athanasiou, 2005), together with a high incidence of graft failure (Minas et al., 2014), restrict their therapeutic appeal.

Adult hMSCs offer an alternative therapeutic strategy due to their ease of isolation, relatively high *ex vivo* growth potential, and trophic effects. Localized injection of hMSCs relieves pain in patients with osteoarthritis (OA) (Mehrabani et al., 2016) and improves cartilage repair scores (Vega et al., 2015; Wong et al., 2013). Moreover, hMSC-seeded collagen scaffolds enhance the healing of avascular meniscal tears (Whitehouse et al., 2017).

Such therapies, however, are restricted by the limited availability of cells, as hMSCs *in situ* only account for ~0.01%–0.0001% of the bone marrow mononuclear cell population (Caplan, 2009). Thus, *ex vivo* expansion is required, with many studies exploiting components of the bone marrow microenvironment to enhance hMSC growth (Kusuma et al., 2017).

Fibroblast growth factor 2 (FGF2) is widely used as an adjuvant to increase hMSC proliferation (Auletta et al., 2011; Gharibi and Hughes, 2012). However, prolonged FGF2 supplementation can adversely affect hMSC stemness (Gharibi and Hughes, 2012). Notably, MSCs expanded with FGF2 yield increasing proportions of differentiated progeny with reduced expression of CD49, STRO-1, CD90, CD105, and CD146 (Hagmann et al., 2013). Also, FGF2 has a short half-life in culture, with ~80% degrading within the first 24 h (Caldwell et al., 2004). FGF2 is therefore supplemented into cultures at supraphysiological levels, which may adversely affect stem cell multipotency (Gharibi and Hughes, 2012). Importantly, hMSCs produce high levels of endogenous FGF2 (Samsonraj et al., 2015), which acts in a paracrine manner to influence mitogenesis when appropriately complexed with particular heparan sulfate proteoglycans (HSPGs) (Titmarsh et al., 2017; Wijesinghe et al., 2017).
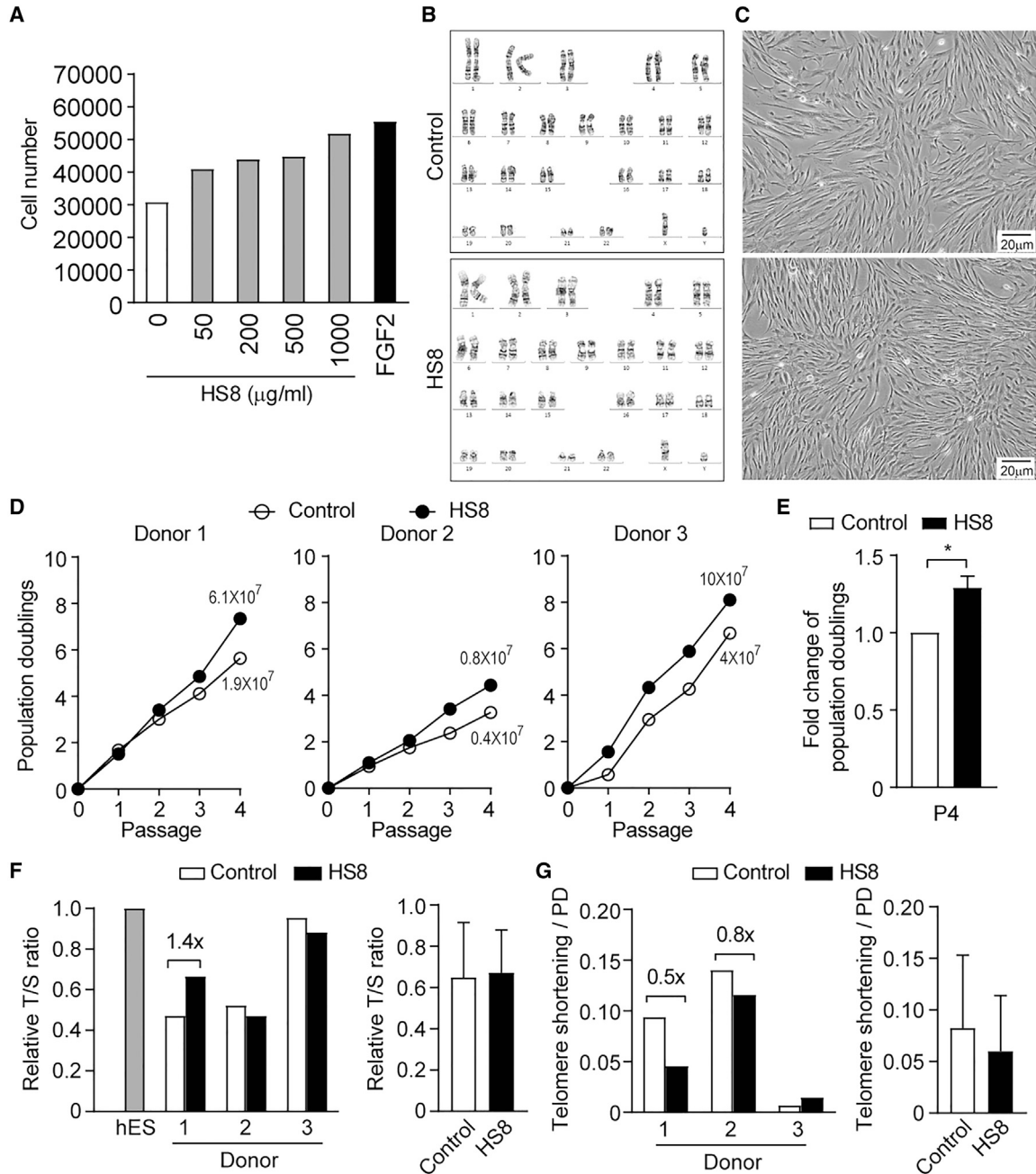
Figure 1. Effect of HS8 on the Growth and Telomere Length of hMSCs

(A) hMSCs (~P5, Lonza) were treated as indicated for 4 days and the number of viable cells determined using the GUAVA Viacount assay (data from a single experiment).

(B) hMSCs (P5, Lonza) were serially passaged with or without HS8 (50 μg/mL) for four passages, and then karyotyped (data from a single experiment).

(C–G) Freshly isolated hMSCs from three donors were cultured with or without HS8 (50 μg/mL) for four passages. The morphology of P4 cells was examined by phase-contrast microscopy; representative images in (C) are from a single experiment. The numbers of hMSCs were counted using a hemocytometer at the end of each passage and the cumulative population doublings calculated (data from a single experiment for each donor); cell numbers at the end of P4 are also indicated (D). After four passages, the fold-change in population doublings of HS8-expanded hMSCs for donors 1–3 in (D) relative to control is shown in (E). Data represent mean ± SD for all donors. The

(legend continued on next page)

HSPGs, consisting of linear HS side chains attached to a core protein, are expressed in nearly all animal tissues (Ori et al., 2008). These HS chains associate with FGFs and their cognate receptors (FGFR1-4) to form trimeric complexes essential for FGF signaling and subsequent cell proliferation and differentiation (Nugent and Edelman, 1992). Rather than supplementing hMSC cultures with supraphysiological levels of exogenous FGF2, we sought to utilize an FGF2-binding heparan sulfate (HS) as a stand-alone culture supplement. We reasoned that such an adjuvant would act to prolong the half-life of endogenously produced FGF2, so sustaining growth-promoting signaling complexes, resulting in increased numbers of hMSCs that maintain their stem cell-like properties (Titmarsh et al., 2017; Wijesinghe et al., 2017).

We have previously employed affinity chromatography using a peptide substrate corresponding to a heparin-binding domain of FGF2 (Wijesinghe et al., 2017) to generate an HS variant with increased FGF2 binding properties. We showed that adult hMSCs culture-supplemented with HS8 generated more cells with stem cell-like activity (Wijesinghe et al., 2017). Here, we show that media supplementation with higher amounts of HS8 results in a 2- to 3-fold increase in the number of freshly isolated hMSCs within 2 weeks. These HS8-expanded hMSCs were highly potent and able to regenerate osteochondral defects in both small and large animals, which highlights the potential HS adjuvants have in the formulation of media used to culture hMSCs for therapeutic use.

RESULTS

Proliferation and Telomere Length
To explore the utility of HS8 as a stem cell culture adjuvant, we first assessed the dose-effect of HS8 on hMSCs. The data showed a dose-dependent effect of HS8 on cell number, highlighting that 50 μg/mL or greater amount of HS8 increased cell proliferation (Figure 1A). HS8 at 1,000 μg/mL exerted a proliferative effect similar to FGF2 at 2.5 ng/mL (Figure 1A). Over multiple passages with 50 μg/mL HS8, cells displayed no discernible chromosomal aberration (Figure 1B).

We next sought to assess the response of freshly isolated hMSCs to HS8. Over 2 weeks of culture with HS8 (50 μg/mL), cells retained a typical, spindle-shaped morphology (Figure 1C). Irrespective of donor, HS8 supplemented into hMSC cultures resulted in ~2.6-fold more cells over the control (Figure 1D), with significantly more population doublings (p < 0.05, Figure 1E).

As increased cellular proliferation can result in accelerated telomere loss (Samsonraj et al., 2015), we examined the effect of HS8 on telomere length. hMSCs supplemented with HS8 for four passages have the same, or even longer telomeres, despite their having undergone more population doublings (Figure 1F). Cells from two out of three donors had less telomere shortening per population doubling (Figure 1G).

Clonogenicity and Surface Marker Expression
With a higher dose (50 μg/mL) of HS8 than that in our previous study (Wijesinghe et al., 2017), MSC colony-forming ability was not adversely affected (Figures 2A and 2B). Instead, for one donor (donor 3), HS8 supplementation resulted in a 3.6-fold higher colony-forming ability (Figure 2A).
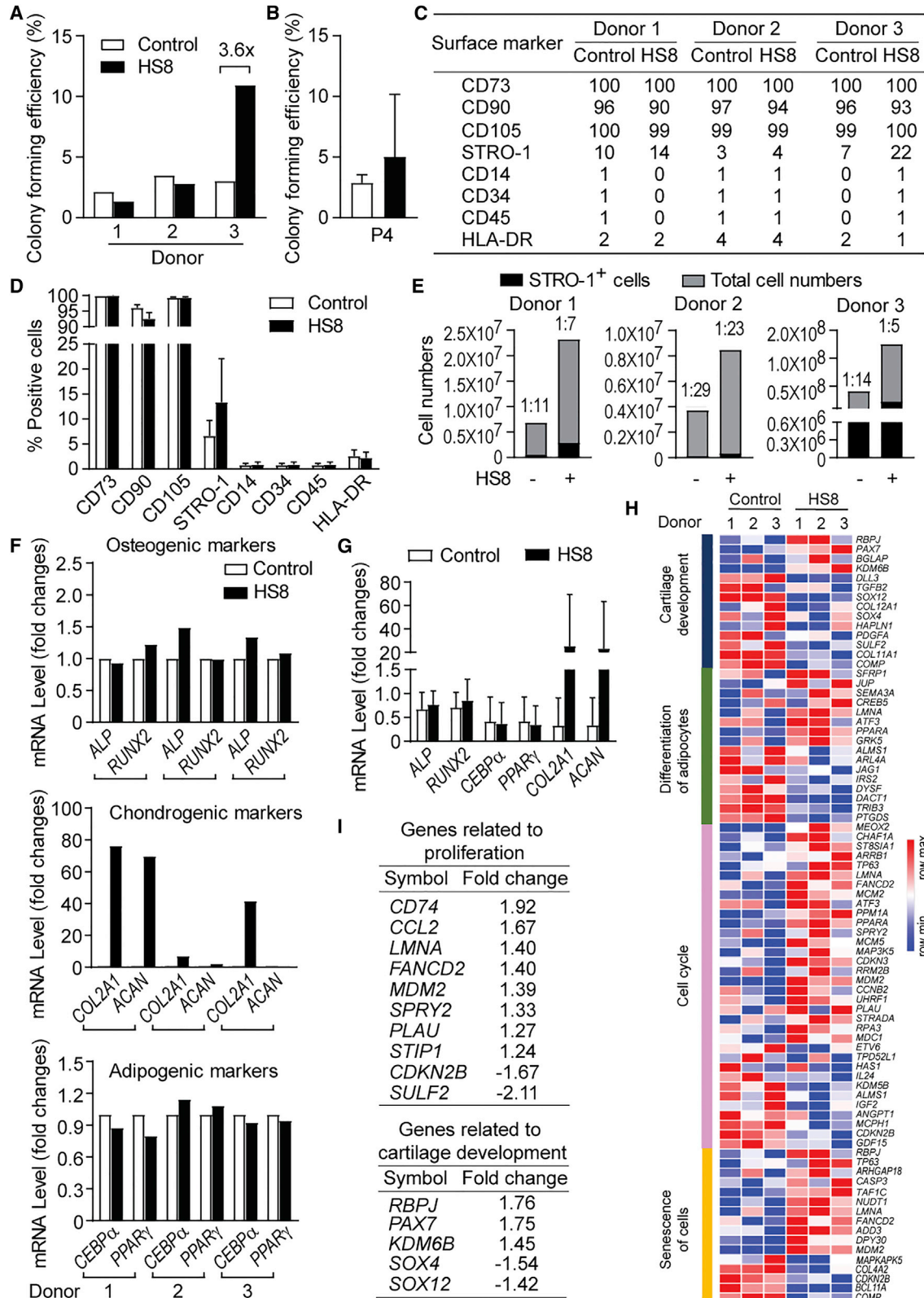
Next, we assessed the hMSCs using a panel of surface markers endorsed by the International Society for Cellular Therapy (ISCT). Expression levels were within the expected ranges (Figures 2C and 2D). Cells were also profiled for the expression of STRO-1, a cell surface biomarker present on all clonogenic hMSCs (Gronthos et al., 1994; Walsh et al., 2000). In two out of three donors, hMSCs expanded for four passages with HS8 demonstrated a robust increase in STRO-1 expression; cells from donor 3 had an ~3-fold higher expression (Figure 2E), a result that mirrored their increased colony-forming ability (Figure 2A). In contrast, STRO-1 expression in hMSCs from donor 2 was minimally affected by HS8 supplementation, suggesting dose- and donor-dependent effects.

Multipotentiality
The multipotency of culture-expanded hMSCs was determined after lineage-specific induction. The mRNA expression of transcripts typical for the bone, fat, and cartilage lineages were not adversely affected by HS8 supplementation (Figures 2F and 2G), despite the cells having been through more population doublings. Although hMSCs from donors 2 and 3 expressed lower mRNA transcripts for chondrogenic markers than donor 1 (Figure 2F), osteochondral healing was greater when these cells were transplanted into defects (Figure 4A). This might be due to the varying nature of mRNA transcript expression and the fact that their levels are not always proportional to protein expression (Tian et al., 2004).

telomere length of P4 cells was analyzed using a PCR-based assay (F), left panel, data from a single experiment for each donor, and the mean telomere length ± SD for all donors presented in (F), right panel. The telomere shortening during each population doubling is plotted in (G), left panel, data from a single experiment for each donor. The mean change ± SD for all donors is in (G), right panel. See also Figure S6.

A

B

C

Surface marker	Donor 1		Donor 2		Donor 3	
	Control	HS8	Control	HS8	Control	HS8
CD73	100	100	100	100	100	100
CD90	96	90	97	94	96	93
CD105	100	99	99	99	99	100
STRO-1	10	14	3	4	7	22
CD14	1	0	1	1	0	1
CD34	1	0	1	1	0	1
CD45	1	0	1	1	0	1
HLA-DR	2	2	4	4	2	1

D

E

F

G

H

I

Genes related to proliferation

Symbol	Fold change
CD74	1.92
CCL2	1.67
LMNA	1.40
FANCD2	1.40
MDM2	1.39
SPRY2	1.33
PLAU	1.27
STIP1	1.24
CDKN2B	-1.67
SULF2	-2.11

Genes related to cartilage development

Symbol	Fold change
RBPJ	1.76
PAX7	1.75
KDM6B	1.45
SOX4	-1.54
SOX12	-1.42

(legend on next page)

The *in vitro* analyses collectively show that the naive hMSC phenotype was maintained with HS8 supplementation at doses up to 50 μg/mL.

Gene Expression Profiling

When hMSCs were expanded for four consecutive passages in HS8-supplemented (50 μg/mL) medium, their expression profiles became distinct (Figure S1A). Hierarchical clustering based on the differentially expressed genes revealed that the expression pattern of HS8-treated hMSCs from donors 1 and 3 was separable from their control, although cells from donor 2 were not (Figure S1A).

A heatmap of hierarchical clustering-by-function highlighted that groups of genes linked to cartilage development, cell cycle, adipogenic differentiation, and cellular senescence were most affected (Figure 2H). In total, 274 genes were upregulated and 304 downregulated in HS8-expanded hMSCs (Figure S1B). Among those upregulated, there was a group (*CD74*, *CCL2*, *FANCD2*, *MDM2*, *SPRY2*, *PLAU*, *STIP1*, and *LMNA*) known to drive cell cycling and prevent aging (Figure 2I, top panel). Genes known to inhibit cell proliferation or induce cellular senescence (*SULF2* and *CDKN2B*) were downregulated (Figure 2I, top panel). Several genes that contribute to cartilage development, including *RBPJ*, *PAX7*, and *KDM6B*, were upregulated, while the anti-chondrogenic genes *SOX4* and *SOX12* were downregulated (Figure 2I, bottom panel).

Healing of Rat Osteochondral Defects

We next evaluated the therapeutic potency of HS8-expanded stem cells *in vivo*. A rat osteochondral defect model was exploited, and tissue regeneration evaluated 12 weeks after hMSC treatment (Figure 3A). Defects left untreated failed to respond consistently, with International Cartilage Repair Society (ICRS) I scores distributed at two extremes—defects with exposed subchondral bone or defects with nearly normal appearance (Figures 3B and 3C). Treatment with carrier alone (fibrin gel) was equally variable. Treatment with hMSCs (±HS8 supplementation)

demonstrated increased healing responses, with 17%–22% of the defects filled with regenerated tissue macroscopically equivalent to normal cartilage (grade I). Most defects treated with carrier alone or left untreated failed to fully regenerate (6% and 0%, respectively; Figure 3C). All treatment groups achieved ∼40%–50% nearly normal healing; however, half of the untreated defects and 17% of defects treated with carrier alone displayed abnormal filling. Only 6% of control hMSCs (MSC^{control}) and none of the HS8-expanded hMSC (MSC^{HS8})-treated defects appeared severely abnormal (Figure 3C). Among the three parameters of the ICRS I score, the degree of repair and integration were consistently higher when defects were treated with hMSCs, particularly MSC^{HS8} (Figure 3D).

Although ICRS II scores varied considerably among defects treated with hMSCs from the different donors, this was reduced when the cells were expanded with HS8 (Figure 4A). When defects were left untreated or treated with fibrin alone, ICRS II median scores <30 were observed, highlighting their low therapeutic effect (Figure 4B). Treatment with hMSCs resulted in ICRS II median scores ≥65. Efficacy was enhanced when MSCs were culture-expanded with HS8 (Figure 4C), with 72% of the defects resulting in ICRS II scores higher than carrier alone, compared with just 56% when treated with MSC^{control} (Figure 4C). Treatment with hMSCs resulted in higher tissue and cell morphology scores, as well as improved matrix content and chondrocyte clustering (Figure 4D). Increased basal integration and tidemark formation, with less subchondral bone abnormality and enhanced repair of mid/deep zones were also evident (Figure 4D). For all of the ICRS II parameters (except for inflammation, calcification, and vascularization scores), scores for treatment with MSC^{HS8} were higher than those for MSC^{control} or carrier alone with less variability (Figure 4D).

Data from O'Driscoll scores supported the improved therapeutic performance of MSC^{HS8} (Figure S2). Analysis via the Pearson correlation coefficient showed that ICRS II and O'Driscoll scores are highly correlated when defects

---

Figure 2. Effect of HS8 on hMSC Properties

(A and B) hMSCs isolated from donors 1, 2, and 3 were serially passaged for four passages. The P4 cells were assessed for clonogenicity with a CFU-F assay (cells from donors 1 and 2 seeded at ∼9 cells/cm^2 and cells from donor 3 seeded at 15 cells/cm^2). Data from a single experiment for each donor (A); mean ± SD for all donors (B).

(C and D) Cell surface antigen expression by flow cytometry (data from a single experiment for each donor (C); mean ± SD for all donors (D).

(E) The number of STRO-1$^+$ cells relative to the total number of hMSCs (data from a single experiment for each donor).

(F and G) The mRNA levels of lineage-specific markers using TaqMan real-time qPCR after cells were induced into osteogenic, chondrogenic, or adipogenic lineages. The fold-change in relative expression units (REUs) of each gene in HS8-expanded hMSCs relative to control is shown in (F), data from a single experiment for each donor. The fold-change in REUs of each gene was normalized to that of control for donor 1 (G), mean ± SD for all donors.

(H) Heatmap of microarray data showing changes in gene expression.

(I) List of genes related to proliferation and cartilage development.

See also Figure S1.
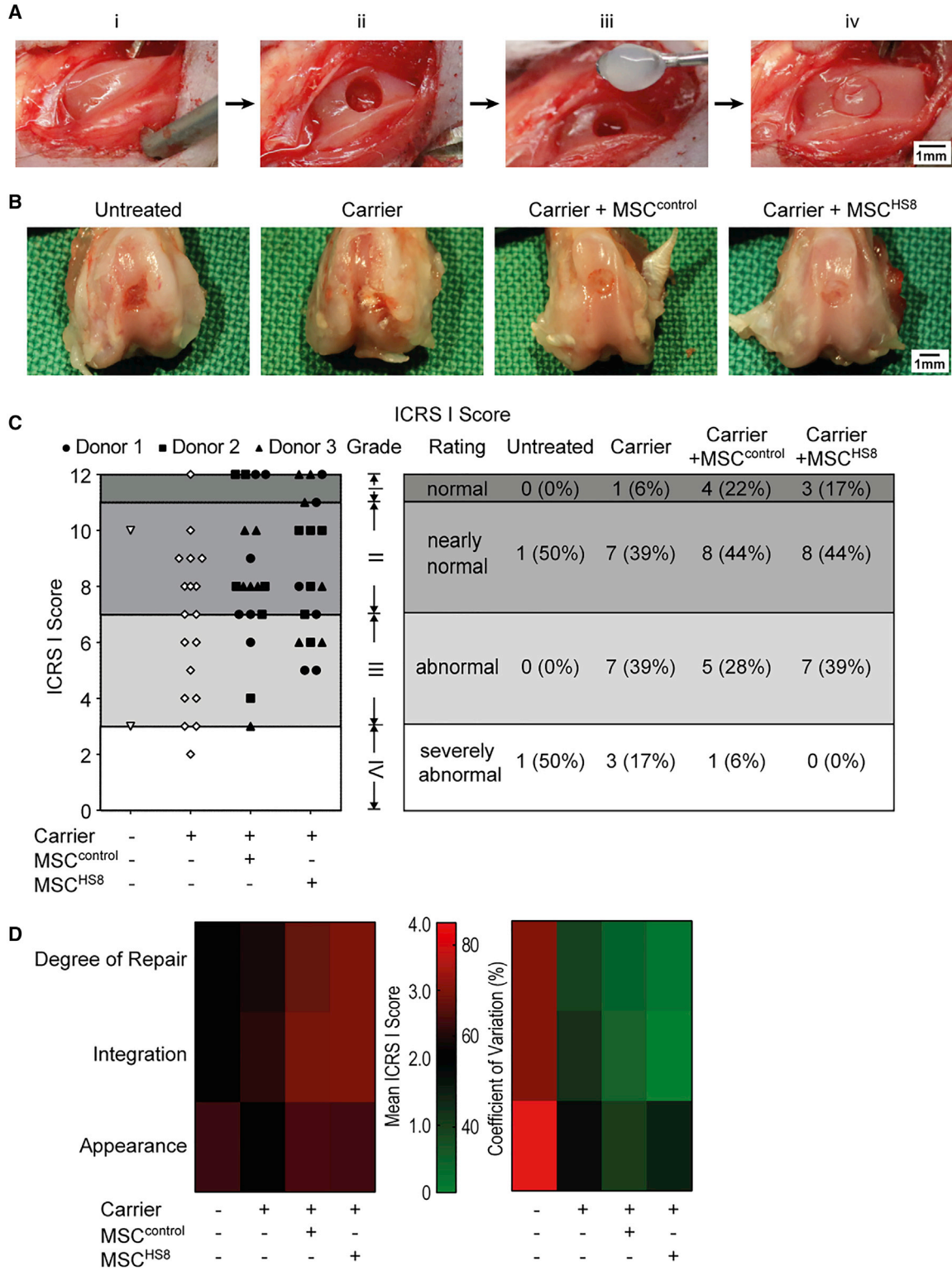
Figure 3. Macroscopic Analysis of Osteochondral Defect Healing in the Rat

(A) Surgical creation of the osteochondral defect in the rat femoral trochlear groove followed by treatment with fibrin gel with/without hMSC therapy. (i) Femoral trochlear groove before the creation of the defect. (ii) Osteochondral defect generated in the middle of the trochlear groove. (iii) hMSCs in fibrin gel. (iv) Defect filled with fibrin gel.

(legend continued on next page)

were treated with MSC[HS8] (p < 0.05, $R^2 = 0.84$), unlike with fibrin alone ($R^2 = 0.35$; Figure S2D).

Histological assessment confirmed the relatively low therapeutic potential of cell-free approaches (Figure S3A), as defects left untreated or treated with fibrin carrier alone resulted in poor filling of both the subchondral and chondral layers, with the regenerated tissue containing large amounts of type I collagen-positive fibrous tissue, and little glycosaminoglycan (GAG). Defects treated with MSC[control] had improved filling of the subchondral bone, with the overlying regenerated chondral layer containing disorganized hyaline cartilage (rich in type II collagen and GAG) and fibrous tissue (type I collagen) (Figure S3A). Defects treated with MSC[HS8] generally had good filling, with the structural integrity of both the subchondral and chondral layers aligned with the surrounding host tissue (Figure S3A). The subchondral region of the defect was filled with bone-like tissue rich in collagen type I beneath a uniform layer of regenerated hyaline cartilage (collagen type II and GAG). To assess the *in vivo* survival of hMSCs in this xenograft model, we used a human mitochondrion-specific antibody. No positively stained human cells were identified in the rat tissues 12 weeks after hMSC implantation (Figure S3B).

Healing of Pig Osteochondral Defects

When MSC[HS8] were used to treat osteochondral defects in immunocompromised pigs (Figure 5A), improved tissue filling was again observed when ~10 million MSC[HS8] were employed, particularly 4 months post-treatment, as confirmed by ICRS I scoring (Figures 5B and 5C). An increased number of defects (17% at 2 months, 84% at 4 months) achieved normal or nearly normal ICRS I scores compared with treatments employing lower numbers (~6 million) of MSC[HS8] (0% at both 2 and 4 months). All defects treated with either fibrin alone, or with ~6 million MSC[HS8], resulted in lower ICRS I scores (abnormal or severely abnormal outcomes), regardless of duration (Figure 5C). Significantly higher ICRS I scores were achieved following treatment with MSC[HS8] (~10 million) when compared with all other conditions at 4 months (Figure 5D). Heatmap analysis of the individual ICRS I parameters revealed that the presence of ~10 million MSC[HS8] improved the degree of repair, integration, and appearance of the defects, with less variability (Figure 5E).
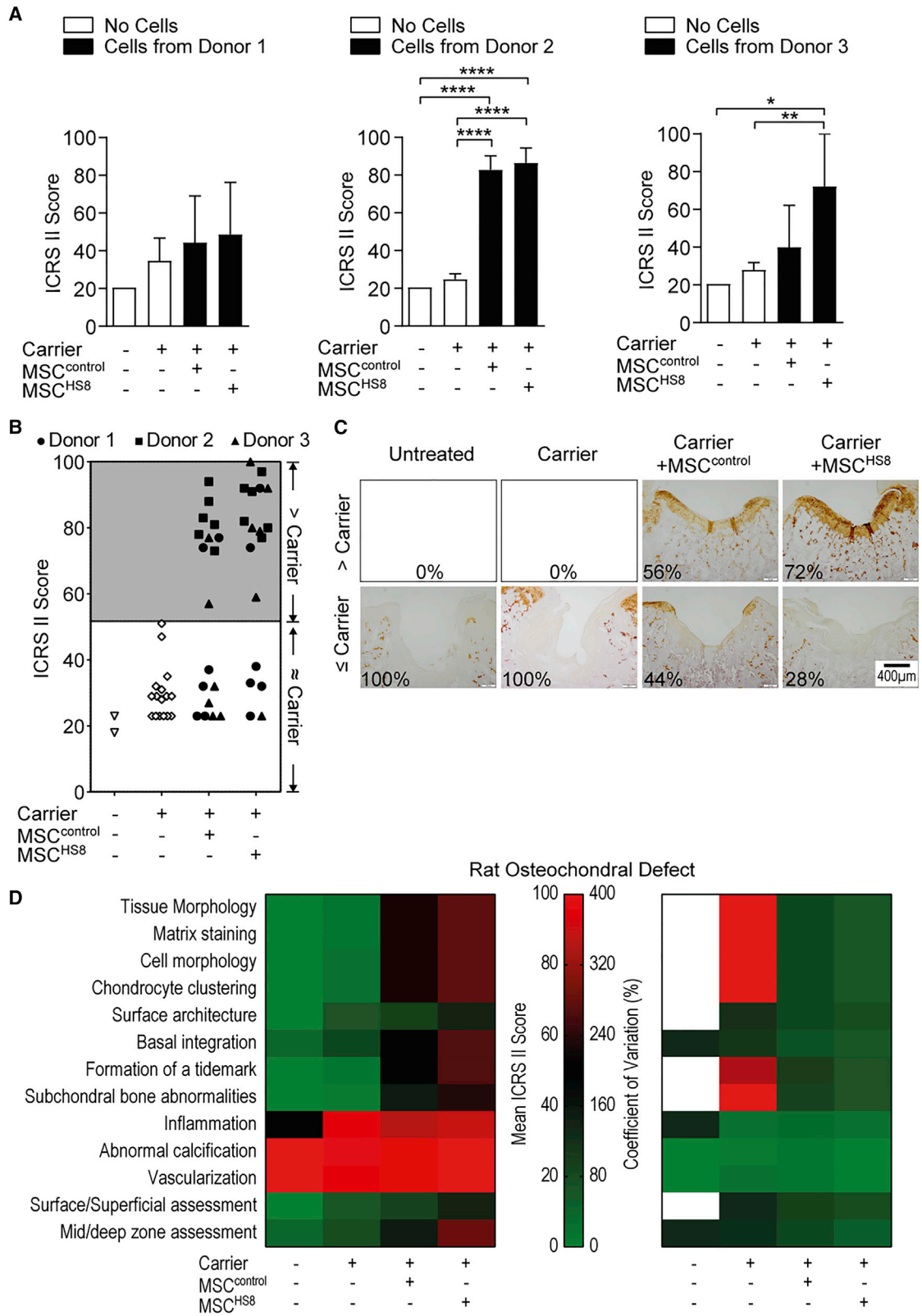
Microscopic assessment of osteochondral healing by ICRS II and O'Driscoll scoring confirmed the therapeutic efficacy of doses of ~10 million MSC[HS8] (Figures 6A, 6B, S4A, and S4B). Such treatment resulted in higher ICRS II (Figure 6B) and O'Driscoll scores (Figure S4B) at both time points, with 67% of the defects performing better than treatment with fibrin carrier alone by 2 months post-treatment; improving to 100% by 4 months (Figure 6C). Only 33% of defects treated with ~6 million MSC[HS8] outperformed fibrin alone by 2 months, and only 17% by 4 months (Figure 6C). Treatment with fibrin carrier alone resulted in limited amounts of bone-like tissue filling the subchondral region and layer of cartilage in the chondral region, irrespective of time post-treatment (Figure S5A). Treatment with ~6 million MSC[HS8] produced slightly more subchondral bone and cartilage by 2 months post-treatment but failed to further improve tissue structure over time (Figure S5A). Treatment with ~10 million MSC[HS8] increased the amount of subchondral bone and cartilage by 2 months, which further improved by 4 months post-treatment (Figure S5A).

Further histological assessment of the individual parameters comprising the ICRS II score, when represented as a heatmap, showed that treatment with ~10 million MSC[HS8] improved tissue responses in most of the parameters (Figure 6D), irrespective of duration. By 4 months post-treatment, parameters related to tissue morphology (more hyaline cartilage than fibrous tissue), matrix content, surface architecture, basal integration, tidemark formation, and subchondral bone (Figure 6E) were all improved. In defects treated with either fibrin gel alone or ~6 million MSC[HS8], minimal restoration of the tidemark reflecting the remodeling of the calcified layer (Havelka et al., 1984) was observed. However, when ~10 million MSC[HS8] were administered to defects, a clear tidemark was observed (Figure S5B, top panel), with substantial amounts of regenerated subchondral bone (Figures 6E and S5B, bottom panel), critical for the successful restoration of the overlying cartilage layer (Gomoll et al., 2010). The tidemark and regenerated subchondral bone together confirm efficacy and are in agreement with the individual parameters comprising the O'Driscoll score (Figure S4C). Consistent with the results seen in the small animal model, outcomes with MSC[HS8] treatment in pigs were also less variable by 4 months post-treatment (Figures S4C and S4D).

(B) Gross appearance of defects with median ICRS I scores after 12 weeks.

(C) Scatterplot of ICRS I scores (each dot represents one defect; filled symbols indicate defects treated with hMSCs and open symbols treatment without hMSCs), and the number and percentage of defects with the corresponding grade for each treatment group. Grade I, 12; grade II, 8–11; grade III, 4–7; grade IV, 1–3.

(D) Heatmap of the mean score and the coefficient of variation for each of the three parameters that comprise the ICRS I score. Carrier, fibrin gel; MSC[control], hMSCs expanded in standard condition; MSC[HS8], hMSCs supplemented with HS8.

A

B ● Donor 1 ■ Donor 2 ▲ Donor 3

C

| | Untreated | Carrier | Carrier +MSC^{control} | Carrier +MSC^{HS8} |

> Carrier: 0% | 0% | 56% | 72%

≤ Carrier: 100% | 100% | 44% | 28%

400μm

D

Rat Osteochondral Defect

Tissue Morphology
Matrix staining
Cell morphology
Chondrocyte clustering
Surface architecture
Basal integration
Formation of a tidemark
Subchondral bone abnormalities
Inflammation
Abnormal calcification
Vascularization
Surface/Superficial assessment
Mid/deep zone assessment

Mean ICRS II Score

Coefficient of Variation (%)

(legend on next page)

MRI corroborated the ICRS I, II, and O'Driscoll scores (Figures 7A and 7B). The Marlovits scores of all 6 defects receiving ~10 million MSC[HS8] for 4 months were greater (Figure 7A, top panel). Further assessment using nine variables pertinent to cartilage repair (Marlovits et al., 2004) highlighted the improvement in cartilage regeneration (Figure 7A, bottom panel). Representative pd_tse_sag_FS sequences show that treatment with ~10 million MSC[HS8] reduced subchondral defect size (dark gray signal) and synovial fluid filling the lesion (white signal) as early as 2 months post-treatment, which improved further after 4 months (Figure 7B). Treatment with ~10 million MSC[HS8] also improved the regeneration of cartilage (light gray signal) overlying the newly repaired subchondral bone in a time-dependent manner (Figure 7B). By 4 months post-treatment, 40%–50% of defects treated with ~10 million MSC[HS8] achieved higher maximum slope and maximum stress, two metrics indicating stiffness and stress resistance (Figure 7C) and significantly improved mechanical properties (Figure 7D). In all cell-based treatments, the tensile stress-strain behavior was non-linear, characteristic of collagen fibrils in articular cartilage that uncoil (toe-in) and then stretch (linear region) under constant strain (Figure 7E). Defects treated with carrier alone failed to resist the same applied strain (flat line) (Figure 7E). Regenerated tissue in defects treated with ~10 million MSC[HS8] had a higher Young's modulus compared with those exposed to ~6 million MSC[HS8], indicating increased stiffness and improved stress resistance.

DISCUSSION

This study confirms the advantage of using heparan GAGs as adjuvants for the culture expansion of naive hMSCs intended for the treatment of osteochondral defects. hMSCs cultured with HS8 have increased population doubling rates, longer telomeres, and higher expression levels of STRO-1. The increased growth rate of MSC[HS8] does not adversely affect the level of key MSC surface markers, clonogenicity, or multipotency. Collectively, these characteristics define a population of cells that are more efficacious for the healing of critical-sized osteochondral defects in rodents, compared with hMSCs cultured without HS8 supplementation. Further testing in a larger animal (porcine) model confirmed that the efficacy of MSC[HS8] could be translated to a more relevant pre-clinical model. We conclude that MSC[HS8] warrants further development as a clinical option for patients with an osteochondral injury.

Over the past decade, the general safety and efficacy of hMSCs for the treatment of cartilage damage have been demonstrated in numerous registered human clinical trials (Wang et al., 2017). In parallel, *ex vivo* strategies have been trialed to narrow the gap between the relatively sparse number of hMSCs in a bone marrow aspirate and the numbers needed for therapy ($\sim10^6$ to 10^{10}) (Lambrechts et al., 2016). For such purposes, stirred microcarrier/bioreactor systems have been developed to provide high surface-to-volume ratios for cell attachment. When expanded under these conditions, MSC population doubling time (PDT) ranges from 40 to 120 h (Heathman et al., 2015; Lambrechts et al., 2016; Rafiq et al., 2013) (Figure S6). Notably, assessments of stemness in these studies were mostly limited to the minimal criteria established by the ISCT (Dominici et al., 2006; Heathman et al., 2015; Lambrechts et al., 2016; Rafiq et al., 2013; Shekaran et al., 2016). In contrast, using 2D monolayer culture, we show that MSC[HS8] have PDT ranging from 40 to 80 h (mean = 60 h), a result closer to the PDT of fetal MSCs (~43 h), a phenotypically younger and more naive population of cells (Shekaran et al., 2016) (Figure S6). Gene expression profiling suggests that HS8 supplementation positively regulates a molecular network that promotes cell proliferation and prevents cellular senescence; in particular, *SULF2* expression is reduced in MSC[HS8]. *SULF2* encodes 6-O-endosulfatase, an enzyme that reduces 6-O-sulfated heparan sulfate chains and accelerates tissue aging (Yamada et al., 2017). The 6-O-sulfation of HS chains is required for the binding of HS to FGFR1 and the establishment of an active FGF2-signaling complex (Wang et al., 2004). Notably, HS8 is enriched with 6-O-sulfated moieties (Wijesinghe et al., 2017). Thus, supplementation with HS8 may help to sustain FGF signaling by providing a culture microenvironment enriched in 6-O-sulfated HS. Further mechanistic studies are needed to better understand the relationship between exogenous supplementation with HS and *SULF2* expression.

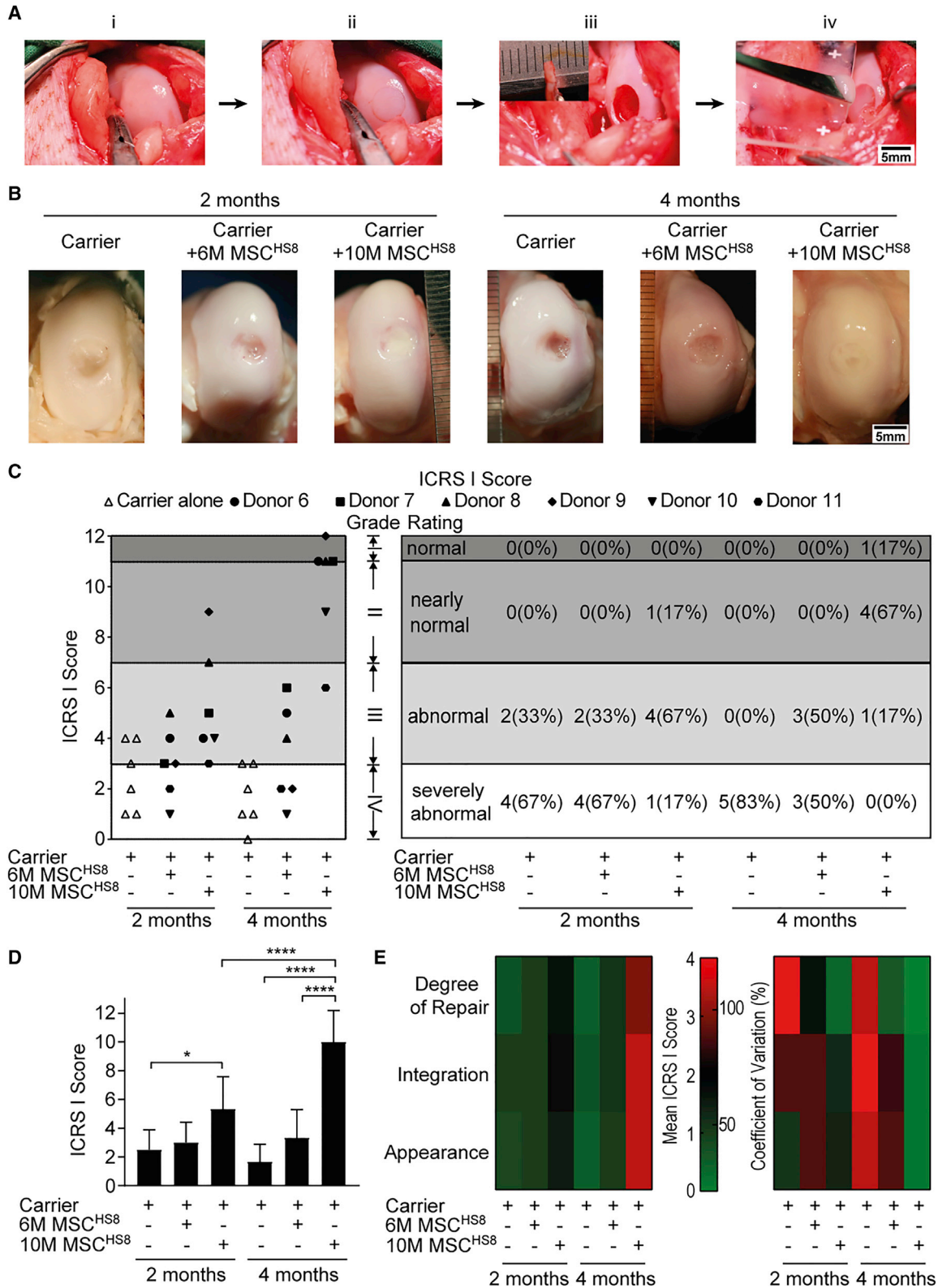**Figure 4. ICRS II Scores of Rat Osteochondral Defect Healing**
(A) ICRS II scores for defects treated with hMSCs from each donor. Data (n = 6 defects) presented as mean ± SD.
(B) ICRS II scores presented as a scatterplot. Defects with scores in the shaded area achieved higher healing scores than those treated with carrier alone. Defects with scores in the clear area manifested scores similar to fibrin alone.
(C) Collagen type II immunohistochemical staining of defects achieving the median ICRS II score in each treatment group. Percentages represent values for defects with scores more than carrier (>carrier), or equal to and lower than carrier (≤Carrier). Carrier, fibrin gel; MSC[control], hMSCs expanded in standard condition; MSC[HS8], hMSCs supplemented with HS8.
(D) Heatmap of the mean score and the coefficient of variation for each parameter of the ICRS II score.
See also Figures S2 and S3 and Table S1.

A

i → ii → iii → iv

B

2 months | 4 months

Carrier | Carrier +6M MSC^{HS8} | Carrier +10M MSC^{HS8} | Carrier | Carrier +6M MSC^{HS8} | Carrier +10M MSC^{HS8}

C

ICRS I Score

△ Carrier alone ● Donor 6 ■ Donor 7 ▲ Donor 8 ◆ Donor 9 ▼ Donor 10 ● Donor 11

Grade Rating

normal	0(0%)	0(0%)	0(0%)	0(0%)	0(0%)	1(17%)
nearly normal	0(0%)	0(0%)	1(17%)	0(0%)	0(0%)	4(67%)
abnormal	2(33%)	2(33%)	4(67%)	0(0%)	3(50%)	1(17%)
severely abnormal	4(67%)	4(67%)	1(17%)	5(83%)	3(50%)	0(0%)

Carrier	+	+	+	+	+	+
6M MSC^{HS8}	-	+	-	-	+	-
10M MSC^{HS8}	-	-	+	-	-	+
	2 months			4 months		

D

ICRS I Score

Carrier	+	+	+	+	+	+
6M MSC^{HS8}	-	+	-	-	+	-
10M MSC^{HS8}	-	-	+	-	-	+
	2 months			4 months		

E

Degree of Repair

Integration

Appearance

Mean ICRS I Score

Coefficient of Variation (%)

Carrier	+	+	+	+	+	+
6M MSC^{HS8}	-	+	-	-	+	-
10M MSC^{HS8}	-	-	+	-	-	+
	2 months	4 months				

(legend on next page)

FGF2, the affinity-target for HS8 (Wijesinghe et al., 2017), is known to induce STRO-1 expression in stem cells (Morito et al., 2009). Cell surface expression of STRO-1 is directly correlated with clonogenicity, tissue homing, and angiogenic potential (Simmons and Torok-Storb, 1991). Freely diffusible HS8 competes with endogenous HSPGs to release bound FGF2, so maximizing its bioavailability (Titmarsh et al., 2017). This increased bioavailability prolongs FGF2 signaling (Wijesinghe et al., 2017), which may help explain the higher expression of STRO-1 in MSC^{HS8}. Also, our data show that hMSCs with the lowest levels of STRO-1 proliferate more slowly than those with higher STRO-1 levels and respond least favorably to HS8 supplementation. This variable response to HS8 may be due to the level of endogenous FGF2 in each of the donor cells, a subject of continuing investigation in our laboratory.

Our data show reduced telomere shortening in hMSCs exposed to HS8 over multiple passages. Telomere length is associated with proliferative capacity, with shortening rep is mediated by telomerase activity (Greider and Blackburn, 1989). FGF2 increases telomerase activity and telomere length in hESCs through the Wnt/β-catenin pathway (Zou et al., 2016). Our finding parallels the general beneficial effect of FGF2 on the longevity of stem cells (Coutu and Galipeau, 2011) and further supports the assertion that HS8 supplementation supports a population of highly proliferative, yet relatively naive hMSCs. However, as telomerase is absent in both control or HS8-expanded hMSCs (data not shown), consistent with previous studies showing low-to-nil levels of telomerase in this cell type (Hiyama and Hiyama, 2007; Zimmermann et al., 2003), HS8 might exert its effects through a telomerase-independent mechanism.

To determine whether these *in vitro* benefits translated to enhanced *in vivo* efficacy, MSC^{HS8} was administered into an osteochondral wound in both small and large animal models. The study in rodents demonstrated that MSC^{HS8} could markedly improve healing scores. Gene profiling of MSC^{HS8} showed expression of products favorable to cartilage development, which may contribute to the molecular mechanism involved in their enhanced therapeutic efficacy. Results from the micropigs further supported this.

No adverse events or pathology were observed in pigs treated with these cells (data not shown). MSC^{HS8} significantly improved the healing of both hyaline cartilage and the underlying subchondral bone tissue, a result supported by both MRI and the improved functional recovery. Moreover, the regenerated chondral layer in the porcine defects treated with MSC^{HS8} demonstrated a significant increase in Young's modulus and the ability to withstand stress.

We note that the animal models used in this study were immunocompromised, and that tissue regeneration in these animals may differ from their more immunocompetent counterparts. However, to perform the current study in immunocompetent animals would have required the use of HS8-expanded rat or pig MSCs. Given that the rationale for the study was to determine the therapeutic potency of hMSCs culture expanded with HS8 as a prelude to future clinical trials, we feel justified in the use of immunocompromised animals.

In conclusion, we applied an affinity-purified HS variant that targets FGF2 to enhance the biological properties of hMSCs. Our work demonstrates that HS8 supplementation helps to preserve stem cell characteristics. Importantly, local administration of MSC^{HS8} significantly improved the healing of large osteochondral defects in both rodents and micropigs. These data highlight the importance of maintaining the quality of stem cells during *ex vivo* expansion and provides support for the further development of niche-mimicking culture systems to cultivate highly potent naive stem cells for therapeutic use.

EXPERIMENTAL PROCEDURES

HS8 Manufacture

The HS variant with enhanced affinity for FGF2 (HS8) was isolated by affinity chromatography as described previously (Murali et al., 2013; Wijesinghe et al., 2017) with modifications (see details in Supplemental Experimental Procedures).

Isolation and Culture of hMSCs

Bone marrow (50 mL) was withdrawn from the iliac crest of 11 young, healthy male donors aged 21–30 years, under local anesthesia following informed consent and strict adherence to ethical

---

**Figure 5. Macroscopic Analysis of the Pig Osteochondral Defect Healing**
(A) Surgical procedure to create and treat osteochondral defects in the femoral condylar groove of micropigs. (i) Intact medial femoral condyle; (ii) the size and position of the defect; (iii) the defect depth; (iv) filling the defect with fibrin gel (Carrier) with/without ~6 million or ~10 million hMSCs cultured with HS8 (~6M MSC^{HS8} and ~10M MSC^{HS8}, respectively).
(B) Gross appearance of defects that achieved the median ICRS I score in each group.
(C) Scatterplot of the ICRS I scores for each treatment, and the number and percentage of defects achieving scores corresponding to a particular grade for each treatment. The score of one defect treated with the carrier alone for 4 months was 0 (non-gradable) and thus was excluded from the rating in the table (right panel).
(D) Bar graph representing mean ± SD of ICRS I scores of six defects.
(E) Heatmap of the mean score and the coefficient of variation for each parameter of the ICRS I score.
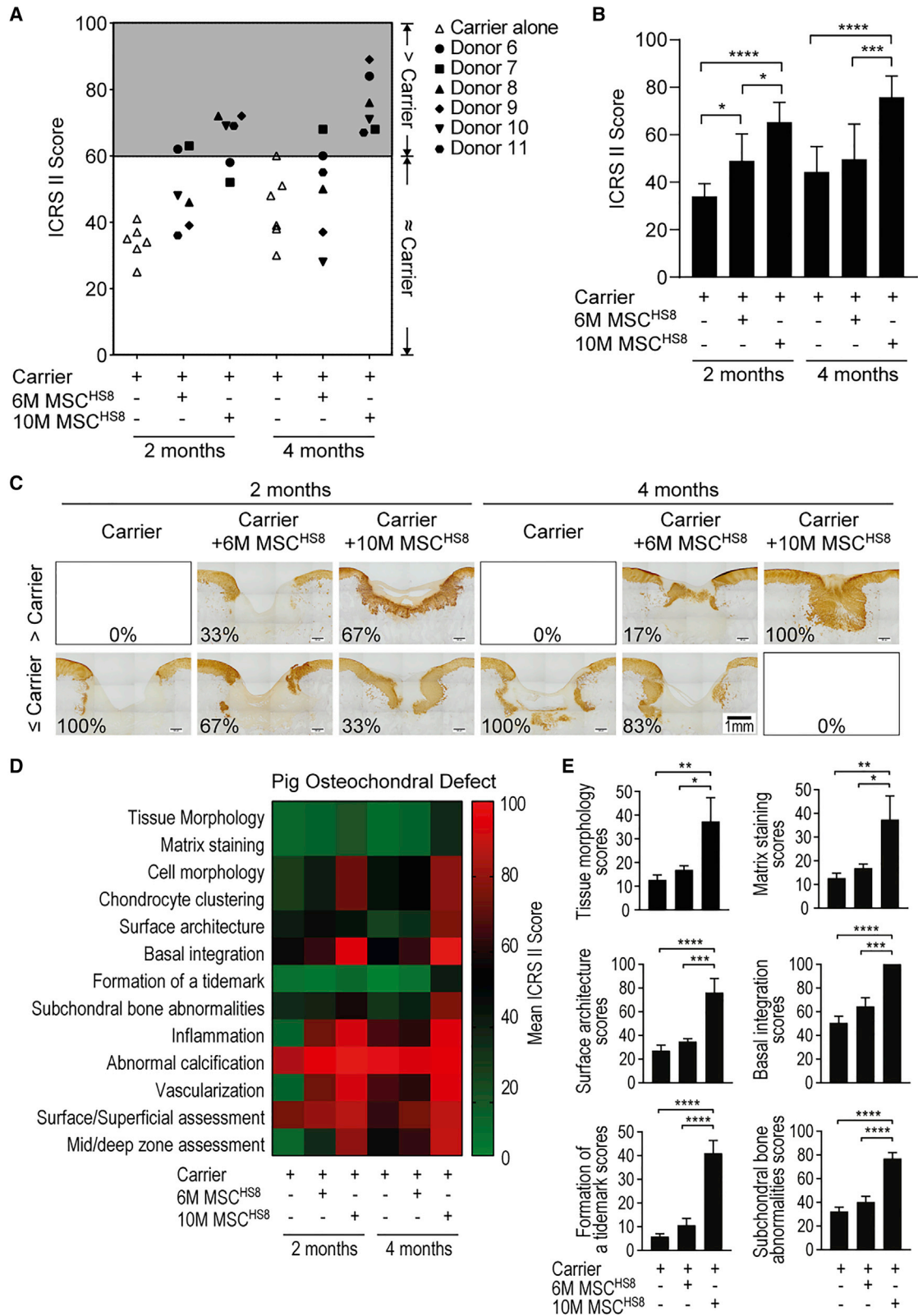
(legend on next page)

guidelines (NHG DSRB ref no. 2013/00737). MSCs were isolated and cultured according to our standard protocols (see details in Supplemental Experimental Procedures).

GUAVA Viacount Assay

To titrate the effective dosage of HS8, human bone marrow-derived MSCs (Lonza, Switzerland) were seeded at 5,000 cells/cm^2 in triplicate and allowed to adhere overnight. Cells were treated with HS8 at the indicated doses or with 2.5 ng/mL FGF2 (R&D Systems, MN, USA) and viable cells counted using the GUAVA Viacount Program as described previously (Ling et al., 2016).

Karyotyping

Human bone marrow-derived MSCs (Lonza), serially passaged 4 times with or without 50 μg/mL HS8, were sent for karyotyping at the Cytogenetics Laboratory of the Singapore General Hospital. A sample with at least two cells with abnormal chromosomes would be reported as an abnormal karyotype.

Population Doubling Calculation

Population doubling (PD) was calculated according to the formula: $N_h/N_s = 2^{PD}$, where N_h is the number of cells harvested and N_s is the number of cells seeded (Zou et al., 2016). The PD at any particular time point was the cumulative population doublings of all previous passages. PDT was calculated using the formula: PDT = t × log(2)/log(number of cells harvested/number of cells seeded), where t is the hours counted from the time point when cells were seeded until the time point when cells were harvested (Lechanteur et al., 2016).

Telomere Length and CFU-F Assay

Following serial passaging with or without HS8 (50 μg/mL), the telomere length of hMSCs was determined using a qPCR method as described previously (Ling et al., 2016), and the clonogenicity determined by a colony-forming unit-fibroblastic (CFU-F) assay (Pochampally, 2008). For CFU-F quantification, cells were cultured for 14 days before crystal violet staining was performed, and the number of discreet colonies counted. Colony-forming efficiency is represented as the colony number divided by the number of cells seeded, expressed as a percentage.

Flow Cytometry

Sub-confluent cells were detached using TrypLE Select (Thermo Fisher Scientific, MA, USA) and washed with PBS. The levels of cell surface markers recommended by ISCT were determined with MSC phenotyping kit (Miltenyi Biotec, Germany) as instructed. The levels of HLA-DR and STRO-1 on the cell surface were determined as described previously (Samsonraj et al., 2015). The number of stained cells was determined using FACSCanto II (BD Biosciences, CA, USA), and the data analyzed using FACSDiva software (BD Biosciences) by gating at <2% of the isotype control.

Multilineage Differentiation and TaqMan Real-Time qPCR Analysis

Serially passaged hMSCs were differentiated into the osteogenic, chondrogenic, or adipogenic lineages, and the expression level of lineage-specific markers analyzed using the TaqMan real-time PCR approach as described previously (Ling et al., 2015, 2016). Primers and probes were all pre-designed by Applied Biosystems (Thermo Fisher Scientific).

Microarray Analysis

The RNA extraction, cRNA generation, and hybridization onto HumanHT-12 v4.0 (Illumina, CA, USA), followed by scanning, were performed as described previously (Sathiyanathan et al., 2017). The background-subtracted data generated by GenomeStudio (Illumina) was read on R with the Bioconductor packages "limma" and "illuminaio." Comparative analysis of the normalized (function "neqc()") donor-corrected data found differentially expressed genes which were filtered by applying a statistical significance of $p_{adj} \leq 0.05$. Gene ontology of the resultant entity list was performed by Ingenuity Pathway Analysis (QIAGEN, Germany). A heatmap of the differentially expressed genes involved in the four most significant biological processes relevant to MSC function that are predicted to increase/decrease in the analyzed data were constructed on Morpheus (https://software.broadinstitute.org/morpheus/). The acccession number for the data reported in this paper is GEO: GSE131164.

In Vivo Study of Osteochondral Defect Healing

All protocols were approved by the Institutional Animal Care and Use Committee (IACUC) of the National University of Singapore (NUS IACUC: 141/12). Details of animal usage are provided in Table S1. For testing in small animals, 37 NIH nude rats (female, 10 weeks old, ~150 g in weight) were purchased from Taconic Biosciences (USA). One rat was randomly chosen as the intact animal control (no surgery performed). For the remaining 36 rats, surgery was performed as per our published procedure (Liu et al., 2011)

Figure 6. ICRS II Scores of Osteochondral Defect Healing in the Pig

(A) Scatterplot of ICRS II scores following treatment with either carrier alone or ~6 million (~6M MSC^{HS8}) or ~10 million (~10M MSC^{HS8}) cells cultured with HS8. Defects indicated in the shaded area achieved higher scores than the best responder from the carrier (fibrin gel) alone. Scores of defects in the clear area are similar to those for treatment with fibrin gel alone.

(B) Bar graph represents mean ± SD of ICRS II scores of six defects.

(C) Collagen type II immunohistochemical staining of defects achieving the median ICRS II score in each treatment group. Percentages represent values for defects with scores more than carrier (>carrier), or equal to and lower than carrier (≤carrier).

(D) Heatmap of the mean score and the coefficient of variation for each parameter of the ICRS II score.

(E) Scores for the individual parameter of the ICRS II score significantly altered by MSC treatment. Data presented as mean ± SD of scores of six defects.

See also Figures S4 and S5 and Table S1.
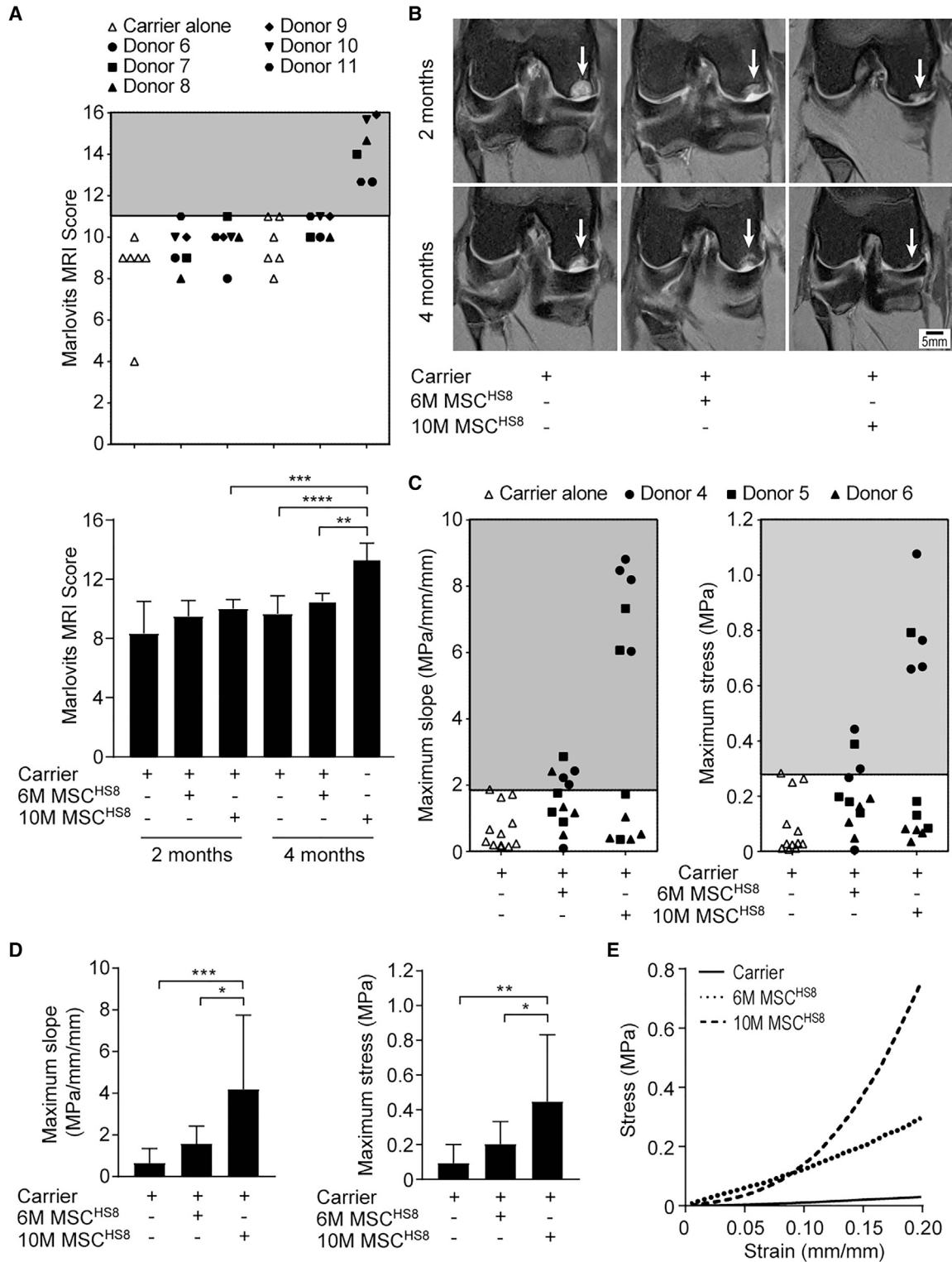
Figure 7. MRI Analysis and Biomechanical Testing of Osteochondral Defects

Defects treated with either carrier alone or ~6 million (~6M MSC^HS8) or ~10 million (~10M MSC^HS8) cells cultured with HS8.

(A) Scatterplot of MRI scores following treatment with hMSCs from different donors (top panel). Data presented as mean ± SD of scores of six defects (bottom panel).

(legend continued on next page)

with some modifications (see details in Supplemental Experimental Procedures). For testing in large animals, surgery was performed on 45 micropigs (female, ~2 years old, ~27 kg in weight) supplied by Prestige BioResearch, Singapore, as per our published procedure (Pochampally, 2008) with some modifications (see details in Supplemental Experimental Procedures).

Biomechanical Studies

Biomechanical testing (Instron 5543, MA, USA) was performed in micropig samples at four fixed positions across the surface of the defect. Before testing, samples were positioned in a holder that allowed for horizontal alignment of the cartilage surface with the probe. Mechanical properties were assessed using cell-load ranges of up to 10 N as applied through a 2.0-mm diameter, plane-ended indenter (Captan Permaflow, Gardena, CA, USA). A pre-load of 0.01 MPa was applied for 30 s to the sample surface (area of 3.14 mm^2), and displacement of the sample surface to 0.2 mm measured at a rate of 0.1 mm/min. Young's modulus was determined after 4 min, using a Poisson ratio of 0.45 (Wang et al., 2017). Data were analyzed with Bluehill 3 software (Instron).

Histology

Specimens were fixed, decalcified, and sectioned as described previously (Hui et al., 2013). A control specimen was taken from the right knee of the intact rat due to the use of a bilateral defect model. Because the porcine model utilized a unilateral defect model, an intact control specimen was harvested from one of the uninjured contralateral joints. Histochemical staining was performed on 5-μm-thick sections. Masson-Trichrome (Sigma-Aldrich, MO, USA) staining was used to mark soft tissue/cartilage (green) and the calcified tissue/subchondral bone (red), and Toluidine blue (Sigma-Aldrich) was used to stain GAGs as purple. Collagen I/II immuno-staining (Sigma-Aldrich) was also applied. Defect areas were defined by comparing images of normal articular surfaces with images of unrepaired defects. The data were quantified by grid counting, and qualitative analysis of the neo-tissue was based on both cell morphology and ECM content. ICRS II scores were determined using 14 parameters (Mainil-Varlet et al., 2010). O'Driscoll scores (Brittberg and Winalski, 2003) were also assessed.

MRI

MRI was performed on the micropig samples in a 3T Siemens Magnetom Skyra with dedicated knee coil and the software version of E11 (Siemens, Erlangen, Germany). The knees were scanned with the sequences of pd_tse_sag_FS (orientation of 156; resolution matrix of 256 × 205; field of view [FoV] read of 350 mm; FoV phase 100%; slice thickness 2 mm; repetition time = 7.8 ms; time to echo = 3.69 ms; fat suppression 35). For each sample, 3–4 sections were cut through the defects and the section running through the center of the defect was selected as the representative image. Experienced musculoskeletal radiologists evaluated the healing using the scoring system established by Marlovits (Hui et al., 2013).

Statistical Analysis

Unless indicated, results are reported as the mean ± SD for three or more independent experiments. The data were analyzed using GraphPad Prism software (GraphPad, CA, USA), followed by two-tailed Student's t test if the comparison was between two groups, or one-way ANOVA if the comparison was among three or more groups, except when two-way ANOVA was used to analyze the data from the histological study. Linear regression was performed to determine the association between ICRS II and O'Driscoll scores. The difference was considered significant when $p < 0.05$ and represented by asterisks ($*p < 0.05$, $**p < 0.01$, $***p < 0.001$, $****p < 0.0001$).

SUPPLEMENTAL INFORMATION

Supplemental Information can be found online at https://doi.org/10.1016/j.stemcr.2019.12.003.

(B) Representative MRI images for median scores in each group. Arrow indicates the osteochondral defect.

(C–E) Biomechanical testing at 4 months post-treatment. Data are presented as a scatterplot (each dot represents one of the four fix positions on the surface of one defect; filled symbols indicate defects treated with hMSCs and open symbols without hMSCs) (C) and as bar graphs depicting mean ± SD (D). Representative stress-strain curves following treatment (E).

REFERENCES

Auletta, J.J., Zale, E.A., Welter, J.F., and Solchaga, L.A. (2011). Fibroblast growth factor-2 enhances expansion of human bone marrow-derived mesenchymal stromal cells without diminishing their immunosuppressive potential. Stem Cells Int. *2011*, 235176.

Bentley, G., Biant, L.C., Vijayan, S., Macmull, S., Skinner, J.A., and Carrington, R.W. (2012). Minimum ten-year results of a prospective randomised study of autologous chondrocyte implantation versus mosaicplasty for symptomatic articular cartilage lesions of the knee. J. Bone Joint Surg. Br. *94*, 504–509.

Brittberg, M., and Winalski, C.S. (2003). Evaluation of cartilage injuries and repair. J. Bone Joint Surg. Am. *85-A (Suppl 2)*, 58–69.

Caldwell, M.A., Garcion, E., terBorg, M.G., He, X., and Svendsen, C.N. (2004). Heparin stabilizes FGF-2 and modulates striatal precursor cell behavior in response to EGF. Exp. Neurol. *188*, 408–420.

Caplan, A.I. (2009). Why are MSCs therapeutic? New data: new insight. J. Pathol. *217*, 318–324.

Coutu, D.L., and Galipeau, J. (2011). Roles of FGF signaling in stem cell self-renewal, senescence and aging. Aging *3*, 920–933.

Darling, E.M., and Athanasiou, K.A. (2005). Rapid phenotypic changes in passaged articular chondrocyte subpopulations. J. Orthop. Res. *23*, 425–432.

Dominici, M., Le Blanc, K., Mueller, I., Slaper-Cortenbach, I., Marini, F., Krause, D., Deans, R., Keating, A., Prockop, D., and Horwitz, E. (2006). Minimal criteria for defining multipotent mesenchymal stromal cells. The International Society for Cellular Therapy position statement. Cytotherapy *8*, 315–317.

Gharibi, B., and Hughes, F.J. (2012). Effects of medium supplements on proliferation, differentiation potential, and in vitro expansion of mesenchymal stem cells. Stem Cell Transl. Med. *1*, 771–782.

Gomoll, A.H., Madry, H., Knutsen, G., van Dijk, N., Seil, R., Brittberg, M., and Kon, E. (2010). The subchondral bone in articular cartilage repair: current problems in the surgical management. Knee Surg. Sports Traumatol. Arthrosc. *18*, 434–447.

Grande, D.A., Pitman, M.I., Peterson, L., Menche, D., and Klein, M. (1989). The repair of experimentally produced defects in rabbit articular cartilage by autologous chondrocyte transplantation. J. Orthop. Res. *7*, 208–218.

Greider, C.W., and Blackburn, E.H. (1989). A telomeric sequence in the RNA of *Tetrahymena* telomerase required for telomere repeat synthesis. Nature *337*, 331–337.

Gronthos, S., Graves, S.E., Ohta, S., and Simmons, P.J. (1994). The STRO-1+ fraction of adult human bone marrow contains the osteogenic precursors. Blood *84*, 4164–4173.

Hagmann, S., Moradi, B., Frank, S., Dreher, T., Kammerer, P.W., Richter, W., and Gotterbarm, T. (2013). FGF-2 addition during expansion of human bone marrow-derived stromal cells alters MSC surface marker distribution and chondrogenic differentiation potential. Cell Prolif. *46*, 396–407.

Havelka, S., Horn, V., Spohrova, D., and Valouch, P. (1984). The calcified-noncalcified cartilage interface: the tidemark. Acta Biol. Hung. *35*, 271–279.

Heathman, T.R., Glyn, V.A., Picken, A., Rafiq, Q.A., Coopman, K., Nienow, A.W., Kara, B., and Hewitt, C.J. (2015). Expansion, harvest and cryopreservation of human mesenchymal stem cells in a serum-free microcarrier process. Biotechnol. Bioeng. *112*, 1696–1707.

Hiyama, E., and Hiyama, K. (2007). Telomere and telomerase in stem cells. Br. J. Cancer *96*, 1020–1024.

Huang, B.J., Hu, J.C., and Athanasiou, K.A. (2016). Cell-based tissue engineering strategies used in the clinical repair of articular cartilage. Biomaterials *98*, 1–22.

Hui, J.H., Ren, X., Afizah, M.H., Chian, K.S., and Mikos, A.G. (2013). Oligo[poly(ethylene glycol)fumarate] hydrogel enhances osteochondral repair in porcine femoral condyle defects. Clin. Orthop. Relat. Res. *471*, 1174–1185.

Kon, E., Gobbi, A., Filardo, G., Delcogliano, M., Zaffagnini, S., and Marcacci, M. (2009). Arthroscopic second-generation autologous chondrocyte implantation compared with microfracture for chondral lesions of the knee: prospective nonrandomized study at 5 years. Am. J. Sports Med. *37*, 33–41.

Kusuma, G.D., Carthew, J., Lim, R., and Frith, J.E. (2017). Effect of the microenvironment on mesenchymal stem cell paracrine signaling: opportunities to engineer the therapeutic effect. Stem Cells Dev. *26*, 617–631.

Lambrechts, T., Sonnaert, M., Schrooten, J., Luyten, F.P., Aerts, J.M., and Papantoniou, I. (2016). Large-scale mesenchymal stem/stromal cell expansion: a visualization tool for bioprocess comparison. Tissue Eng. Part B Rev. *22*, 485–498.

Lechanteur, C., Briquet, A., Giet, O., Delloye, O., Baudoux, E., and Beguin, Y. (2016). Clinical-scale expansion of mesenchymal stromal cells: a large banking experience. J. Transl. Med. *14*, 145.

Ling, L., Camilleri, E.T., Helledie, T., Samsonraj, R.M., Titmarsh, D.M., Chua, R.J., Dreesen, O., Dombrowski, C., Rider, D.A., Galindo, M., et al. (2016). Effect of heparin on the biological properties and molecular signature of human mesenchymal stem cells. Gene *576*, 292–303.

Ling, L., Tan, S.K., Goh, T.H., Cheung, E., Nurcombe, V., van Wijnen, A.J., and Cool, S.M. (2015). Targeting the heparin-binding domain of fibroblast growth factor receptor 1 as a potential cancer therapy. Mol. Cancer *14*, 136.

Liu, T.M., Guo, X.M., Tan, H.S., Hui, J.H., Lim, B., and Lee, E.H. (2011). Zinc-finger protein 145, acting as an upstream regulator of SOX9, improves the differentiation potential of human mesenchymal stem cells for cartilage regeneration and repair. Arthritis Rheum. *63*, 2711–2720.

Mahmoud, E.E., Kamei, N., Kamei, G., Nakasa, T., Shimizu, R., Harada, Y., Adachi, N., Misk, N.A., and Ochi, M. (2017). Role of mesenchymal stem cells densities when injected as suspension in joints with osteochondral defects. Cartilage *10*, 61–69.

Mainil-Varlet, P., Van Damme, B., Nesic, D., Knutsen, G., Kandel, R., and Roberts, S. (2010). A new histology scoring system for the

assessment of the quality of human cartilage repair: ICRS. Am. J. Sports Med. *38*, 880–890.

Marlovits, S., Striessnig, G., Resinger, C.T., Aldrian, S.M., Vecsei, V., Imhof, H., and Trattnig, S. (2004). Definition of pertinent parameters for the evaluation of articular cartilage repair tissue with high-resolution magnetic resonance imaging. Eur. J. Radiol. *52*, 310–319.

Mehrabani, D., Mojtahed Jaberi, F., Zakerinia, M., Hadianfard, M.J., Jalli, R., Tanideh, N., and Zare, S. (2016). The healing effect of bone marrow-derived stem cells in knee osteoarthritis: a case report. World J. Plast. Surg. *5*, 168–174.

Minas, T., Von Keudell, A., Bryant, T., and Gomoll, A.H. (2014). The John Insall Award: a minimum 10-year outcome study of autologous chondrocyte implantation. Clin. Orthop. Relat. Res. *472*, 41–51.

Morito, A., Kida, Y., Suzuki, K., Inoue, K., Kuroda, N., Gomi, K., Arai, T., and Sato, T. (2009). Effects of basic fibroblast growth factor on the development of the stem cell properties of human dental pulp cells. Arch. Histol. Cytol. *72*, 51–64.

Murali, S., Rai, B., Dombrowski, C., Lee, J.L., Lim, Z.X., Bramono, D.S., Ling, L., Bell, T., Hinkley, S., Nathan, S.S., et al. (2013). Affinity-selected heparan sulfate for bone repair. Biomaterials *34*, 5594–5605.

Nugent, M.A., and Edelman, E.R. (1992). Kinetics of basic fibroblast growth factor binding to its receptor and heparan sulfate proteoglycan: a mechanism for cooperactivity. Biochemistry *31*, 8876–8883.

Ori, A., Wilkinson, M.C., and Fernig, D.G. (2008). The heparanome and regulation of cell function: structures, functions and challenges. Front. Biosci. *13*, 4309–4338.

Pochampally, R. (2008). Colony forming unit assays for MSCs. Methods Mol. Biol. *449*, 83–91.

Rafiq, Q.A., Brosnan, K.M., Coopman, K., Nienow, A.W., and Hewitt, C.J. (2013). Culture of human mesenchymal stem cells on microcarriers in a 5 l stirred-tank bioreactor. Biotechnol. Lett. *35*, 1233–1245.

Samsonraj, R.M., Rai, B., Sathiyanathan, P., Puan, K.J., Rotzschke, O., Hui, J.H., Raghunath, M., Stanton, L.W., Nurcombe, V., and Cool, S.M. (2015). Establishing criteria for human mesenchymal stem cell potency. Stem Cells *33*, 1878–1891.

Sathiyanathan, P., Tay, C.Y., and Stanton, L.W. (2017). Transcriptome analysis for the identification of cellular markers related to trabecular meshwork differentiation. BMC Genomics *18*, 383.

Shekaran, A., Lam, A., Sim, E., Jialing, L., Jian, L., Wen, J.T., Chan, J.K., Choolani, M., Reuveny, S., Birch, W., et al. (2016). Biodegradable ECM-coated PCL microcarriers support scalable human early MSC expansion and in vivo bone formation. Cytotherapy *18*, 1332–1344.

Simmons, P.J., and Torok-Storb, B. (1991). Identification of stromal cell precursors in human bone marrow by a novel monoclonal antibody, STRO-1. Blood *78*, 55–62.

Tian, Q., Stepaniants, S.B., Mao, M., Weng, L., Feetham, M.C., Doyle, M.J., Yi, E.C., Dai, H., Thorsson, V., Eng, J., et al. (2004). Integrated genomic and proteomic analyses of gene expression in mammalian cells. Mol. Cell. Proteomics *3*, 960–969.

Titmarsh, D.M., Tan, C.L., Glass, N.R., Nurcombe, V., Cooper-White, J.J., and Cool, S.M. (2017). Microfluidic screening reveals heparan sulfate enhances human mesenchymal stem cell growth by modulating fibroblast growth factor-2 transport. Stem Cell Transl. Med. *6*, 1178–1190.

Vega, A., Martin-Ferrero, M.A., Del Canto, F., Alberca, M., Garcia, V., Munar, A., Orozco, L., Soler, R., Fuertes, J.J., Huguet, M., et al. (2015). Treatment of knee osteoarthritis with allogeneic bone marrow mesenchymal stem cells: a randomized controlled trial. Transplantation *99*, 1681–1690.

Walsh, S., Jefferiss, C., Stewart, K., Jordan, G.R., Screen, J., and Beresford, J.N. (2000). Expression of the developmental markers STRO-1 and alkaline phosphatase in cultures of human marrow stromal cells: regulation by fibroblast growth factor (FGF)-2 and relationship to the expression of FGF receptors 1-4. Bone *27*, 185–195.

Wang, M., Yuan, Z., Ma, N., Hao, C., Guo, W., Zou, G., Zhang, Y., Chen, M., Gao, S., Peng, J., et al. (2017). Advances and prospects in stem cells for cartilage regeneration. Stem Cells Int. *2017*, 4130607.

Wang, S., Ai, X., Freeman, S.D., Pownall, M.E., Lu, Q., Kessler, D.S., and Emerson, C.P., Jr. (2004). QSulf1, a heparan sulfate 6-O-endosulfatase, inhibits fibroblast growth factor signaling in mesoderm induction and angiogenesis. Proc. Natl. Acad. Sci. U S A *101*, 4833–4838.

Whitehouse, M.R., Howells, N.R., Parry, M.C., Austin, E., Kafienah, W., Brady, K., Goodship, A.E., Eldridge, J.D., Blom, A.W., and Hollander, A.P. (2017). Repair of torn avascular meniscal cartilage using undifferentiated autologous mesenchymal stem cells: from in vitro optimization to a first-in-human study. Stem Cells Transl. Med. *6*, 1237–1248.

Wijesinghe, S.J., Ling, L., Murali, S., Qing, Y.H., Hinkley, S.F., Carnachan, S.M., Bell, T.J., Swaminathan, K., Hui, J.H., van Wijnen, A.J., et al. (2017). Affinity selection of FGF2-binding heparan sulfates for ex vivo expansion of human mesenchymal stem cells. J. Cell. Physiol. *232*, 566–575.

Wong, K.L., Lee, K.B., Tai, B.C., Law, P., Lee, E.H., and Hui, J.H. (2013). Injectable cultured bone marrow-derived mesenchymal stem cells in varus knees with cartilage defects undergoing high tibial osteotomy: a prospective, randomized controlled clinical trial with 2 years' follow-up. Arthroscopy *29*, 2020–2028.

Yamada, T., Kerever, A., Yoshimura, Y., Suzuki, Y., Nonaka, R., Higashi, K., Toida, T., Mercier, F., and Arikawa-Hirasawa, E. (2017). Heparan sulfate alterations in extracellular matrix structures and fibroblast growth factor-2 signaling impairment in the aged neurogenic niche. J. Neurochem. *142*, 534–544.

Zimmermann, S., Voss, M., Kaiser, S., Kapp, U., Waller, C.F., and Martens, U.M. (2003). Lack of telomerase activity in human mesenchymal stem cells. Leukemia *17*, 1146–1149.

Zou, Y., Tong, H.J., Li, M., Tan, K.S., and Cao, T. (2016). Telomere length is regulated by FGF-2 in human embryonic stem cells and affects the life span of its differentiated progenies. Biogerontology *18*, 69–84.

University Library

MINERVA ACCESS

A gateway to Melbourne's research publications

Author/s:
Ling, L; Ren, X; Cao, X; Hassan, ABM; Mah, S; Sathiyanathan, P; Smith, RAA; Tan, CLL; Eio, M; Samsonraj, RM; van Wijnen, AJ; Raghunath, M; Nurcombe, V; Hui, JH; Cool, SM

Title:
Enhancing the Efficacy of Stem Cell Therapy with Glycosaminoglycans

Date:
2020-01

Persistent Link:
http://hdl.handle.net/11343/252532

File Description:
Published version
License: